Supporting Information

Differential Mg^{2+} Deposition on DNA Holliday Junctions Dictates the Rate and Stability of Conformational Exchange

Pratibha Agarwala,[1] Arumay Pal[2]†, Milan Kumar Hazra*[1], and Dibyendu K. Sasmal*[1]

[1]Department of Chemistry, Indian Institute of Technology Jodhpur, Rajasthan 342037, India

[2]School of Biosciences, Engineering and Technology, Vellore Institute of Technology, Bhopal, India

†Present Addresses: Department of Pharmaceutical Sciences, University of Illinois at Chicago, Illinois 60607, United States

Experimental Section:

Materials: Tris-hydroxymethyl aminomethane, Magnesium chloride hexahydrate, Sodium chloride and D-glucose were purchased from Merck. Catalase, Glucose oxidase, Biotinylated BSA, Trolox and all single strand DNAs were purchased from Sigma-Aldrich. Streptavidin was purchased from ThermoFisher. Biotinylated BSA and Streptavidin were dissolved in T50 buffer ((10 mM Tris HCl at pH = 8.0, 50 mM NaCl), filtered, and stored at –20 °C temperature for further use.

Preparation of DNA Holliday Junction:

DNA Holliday junction was prepared by thermal Annealing of four single-strand DNA (ssDNA) in an annealing buffer (10 mM Tris HCl at pH = 8.0, 50 mM NaCl and 15 mM $MgCl_2$, $6H_2O$). The sequence of four single-strand DNAs was given as follows. Cy5 labelled: 5′-Cy5-CCC TAG CAA GCC GCT GCT ACG G-3′, Cy3 labelled: 5′-Cy3-CCG TAG CAG CGC GAG CGG TGG G-3′, Biotin labelled: 5′-Biot-CCC ACC GCT CGG CTC AAC TGG G-3′, Unlabelled: 5′-CCC AGT TGA GCG CTT GCT AGG G-3′. The ratio of Cy3:Cy5:Biotin: Unlabelled DNA strands was taken as 2:1:1:2. Annealing was performed by ramping the temperature of solution from 96 °C to 4 °C at a rate of 0.5 °C per minute in a thermal cycler, and the final annealed Holliday Junction was stored at 4 °C.[1]

Preparation of sample chamber smFRET Experiment:

The quartz slide was thoroughly cleaned using the following steps: i) sonication with 5 N NaOH for 20 minutes, followed by washing the slide with distilled water; ii) then we have sonicated the slides for 20 minutes with acetone; iii) for the surface etching procedure, we sonicated the quartz slides two times with 1 M KOH followed by cleaning with distilled water. Then, the slide was burned for 2 minutes. The cover glass was also cleaned with 1 M KOH solution and burned for 30 seconds. The sample chamber was prepared by assembling a cleaned quartz slide and coverslip using double-sided tape of 0.1 µm thickness.[2]

The sample chamber was incubated with 30 µl of Biotin labelled BSA with a concentration of 1 mg/ml for 5 minutes and then washed two times with T50 buffer. After that, 30 µl of streptavidin with a concentration of 0.2 mg/ml was incubated for 2 minutes and washed to avoid any nonspecific binding. The annealed DNA Holliday junction of 250 pM was incubated for 3 minutes and then washed with an imaging buffer solution called gloxy solution having catalase, glucose oxidase and β-D-glucose and 2 mM of Trolox. Appropriate Mg^{2+} concentration was added to the imaging buffer just before the Experiment.[3]

Home-built Prism-type Total Internal Reflection Fluorescence Microscopy (TIRF):[4]

All Experiments were performed in a homebuilt prism based TIRF setup on the top of Olympus confocal microscopy (FV1000). The donor Cy3 was excited by the CW laser of 559 nm wavelength, and subsequently, the Cy5 (acceptor) was also excited by the fluorescence resonance energy transfer principle. The laser beam was focused on the sample by a biconvex lens of focal length 200 mm. The ray was exposed to the sample in such a way that the incident angle was greater than the critical angle so that it creates total internal reflection, and with a evanescent field of 100-200 nm. Emission signals from both Cy3 and Cy5 were collected by a 100X objective with 1.45 numerical aperture (NA) and then entered into Optosplit-II (4f relay system, Crain Research). In the Optosplit II the emission signal from both the donor and acceptor was separated by a dichroic mirror (Chroma, ZT633rdc-UF2) and collected by the bandpass filter ET585/65m for the donor and ET706/95m for the acceptor. Signals from both donor and acceptor were collected by Electron multiplying charge-coupled device camera (EMCCD, Andor Ixon 897). The movies were recorded using an integration time of 50 ms using an open source software Micromanager[5], and data was processed using the open source code SPARTAN 3.7 software.[6]

FRET efficiency was calculated using the formula[7]

$$E_{FRET} = \frac{I_A(t)}{I_A(t)+I_D(t)\times\frac{\Phi_A\times\eta_A}{\Phi_D\times\eta_D}} = \sim \frac{I_A(t)}{I_A(t)+I_D(t)} \qquad (1)$$

Where $I_A(t)$ and $I_D(t)$ were the intensity of the donor and acceptor respectively, and E_{FRET} was the FRET efficiency. Here, the respective emission quantum yield of the donor and acceptor were represented by Φ_D and Φ_A and donor and acceptor detector efficiency were symbolized by η_D and η_A respectively. We have considered that the correction factor was $\frac{\Phi_A\times\eta_A}{\Phi_D\times\eta_D} = 1$.

Supporting Information Table 1. Time constant and amplitude calculated of the two-point time correlation function obtained from the biexponential fitting function.

Concentration of Mg^{2+}	A_1	τ_1 (s)	A_2	τ_2(s)
50 mM	0.36	0.181	0.64	3.787
200 mM	0.51	5.31	0.49	8.19

The analytical expression of the kinetic rate calculation for N= 3 system: [8]

The Master equation for the N=3 system was

$$\dot{p}_t = Kp(t) = \begin{bmatrix}\dot{p_1}\\ \dot{p_2}\\ \dot{p_3}\end{bmatrix} \equiv \begin{bmatrix}-k_{12}-k_{13} & k_{21} & k_{31}\\ k_{12} & -k_{21}-k_{23} & k_{32}\\ k_{13} & k_{23} & -k_{31}-k_{32}\end{bmatrix}\begin{bmatrix}p_1\\ p_2\\ p_3\end{bmatrix} \qquad (2)$$

where $p(t)$ was the time-dependent macrostate population vector composed of $[p_1, p_2, p_3]$ and the time derivative was represented as $\dot{p}_t$. The 3×3 matrix represented by K, which contains the rate constant kij.

Then, the general solution of the Equation 2 was[8-9]-

$$p(t) = p^{eq} + c_2 e^{\lambda_1 t} + c_2 v_2 e^{\lambda_2 t} \qquad (3)$$

Where the eigenvectors were v_1 and v_2, and eigenvalues λ_1 and λ_2 were given by $\lambda_1 = a + b$, $\lambda_2 = a - b$. Definitions of a and b were:

$$a = \frac{1}{2}(k_{12} + k_{21} + k_{23} + k_{32} + k_{13} + k_{31}) \qquad (4)$$

$$b = \frac{1}{2}[(k_{12} - k_{23})^2 + (k_{13} - k_{32})^2 + (k_{21} - k_{31})^2 + 2k_{12}(k_{13} + k_{21} - k_{31} - k_{32}) + 2k_{13}(k_{31} - k_{21} - k_{23}) + 2k_{23}(k_{21} - k_{31} + k_{32}) - 2k_{21}k_{32} + -2k_{31}k_{32}]^{1/2} \quad (5)$$

To satisfy the detailed, balanced condition, one rate constant must depend on others such that $k_{31} = k_{13}k_{32}k_{21}/k_{23}k_{12}$ (6)

The equilibrium populations $p^{eq} = [p_1^{eq}, p_2^{eq}, p_3^{eq}]$ were obtained by solving Equation 2 with the boundary condition $\dot{p}_t = 0$. This gives the results

$$p_1^{eq} = \{1 + [(k_{12} + k_{13})/k_{21}] + [(1 - k_{31})/k_{21}].(k_{21} + k_{23})(k_{12} + k_{13}) - k_{12}.k_{21}/[(k_{21} + k_{23})k_{31} + k_{32}k_{21}]\}^{-1} \quad (7)$$

$$p_2^{eq} = k_{21}^{-1}.[p_1^{eq}(k_{12} + k_{13}) - p_3^{eq}k_{31}] \quad (8)$$

$$p_3^{eq} = p_1^{eq}.[(k_{21} + k_{23})(k_{12} + k_{13}) - k_{12}k_{21}].[(k_{21} + k_{23})k_{31} + k_{32}k_{21}]^{-1} \quad (9)$$

We have used Equation 4-9 to solve the values of the rate constant k_{ij} in the software Wolfram Mathematica.

Another way to find the rate constant was by solving master Equation 2 in kinetic network model, and we have found the following rate constant for 50 mM and 200 mM Mg^{2+}.

Supporting Information Table 2. The rate constant from the kinetic network model and the numerical calculation

Concentration of Mg^{2+}	**k_{12} (s^{-1})**	**k_{21}(s^{-1})**	**k_{13}(s^{-1})**	**k_{31}(s^{-1})**	**k_{23}(s^{-1})**	**k_{32}(s^{-1})**
50 mM (from kinetic Network Model)	0.15	0.16	0	0.009	0.43	4.84
50 mM (from the Numerical Calculation)	0.08	0.09	0.06	0.22	1.28	4.03
200 mM (from kinetic Network Model)	0.16	0.02	0.003	0.014	0.02	0.09
200 mM (from the Numerical Calculation)	0.06	0.03	0.02	0.08	0.01	0.09

We have checked the rate constant values calculated from the numerical solution of Equation 4-9 in the form of rate matrix given in Equation 2.

Rate Matrix for 50 mM Mg^{2+}

$$K = \begin{bmatrix} -0.1424 & 0.0870 & 0.2240 \\ 0.0784 & -1.3660 & 4.0430 \\ 0.0640 & 1.2790 & -4.2670 \end{bmatrix}$$

The solution of the rate matrix for 50 mM Mg^{2+} Concentration

$\lambda_0 =$ -0.0000

$\lambda_1 = -0.2609$

$\lambda_2 = -5.5145$

Rate Matrix for 200 mM Mg^{2+}

$$K = \begin{bmatrix} -0.0830 & 0.03 & 0.08 \\ 0.06 & -0.044 & 0.09 \\ 0.023 & 0.014 & -0.17 \end{bmatrix}$$

The solution of the rate matrix for 200 mM Mg^{2+}

$\lambda_0 =$ -0.0000

$\lambda_1 =$ -0.107

$\lambda_2 =$ -0.189

Supporting Information Table 3. The sequence of ssDNA with the chain ID used for molecular dynamic simulation.

Chain ID	**Sequence**
A (cyan) (Cy3 labelled in experiment)	5′-CCG TAG CAG CGC GAG CGG TGG G-3′
B (yellow) (Cy5 labelled in experiment)	5′-CCC TAG CAA GCC GCT GCT ACG G-3′
C(Magenta)	5′-CCC AGT TGA GCG CTT GCT AGG G-3′
D(green) (biotin labelled in experiment)	5′-CCC ACC GCT CGG CTC AAC TGG G-3′

We have determined fourth order time correlation function,[8] which was the product of four sequential data points of smFRET trajectories, separated by the time interval $\tau_1, (t_2 - t_1), \tau_2\,(t_3 - t_2), \text{and}\ \tau_3(t_4 - t_3)$.

The fourth-order time correlation function can be calculated as

$$C^{(4)}(\tau_1, \tau_2, \tau_3) = \langle \delta E_{FRET}(0)\delta E_{FRET}(\tau_1)\delta E_{FRET}(\tau_1 + \tau_2)\delta E_{FRET}(\tau_1 + \tau_2 + \tau_3)\rangle \quad (10)$$

The fourth-order time correlation function illustrates the correlation between the interval at τ_1 and τ_3 at a fixed τ_2 value, depending on the weighted observation of each possible time. The fourth-order time correlation function was composed of $(N\text{-}1)^2$ terms, where N represents the number of states present. Here the $A_{n,m}$ represents amplitudes. For an equilibrium system, the principle of a detailed balance Equation was $A_{n,m} = A_{m,n}$ [8]

$$C^4(\tau_1, \tau_3)_{\tau_2\,\text{fixed}} = A_{22}(\tau_2)e^{\lambda_1(\tau_1+\tau_3)} + A_{23}(\tau_2)e^{\lambda_1\tau_1+\lambda_2\tau_3} + A_{32}(\tau_2)e^{\lambda_2\tau_1+\lambda_1\tau_3} + A_{33}(\tau_2)e^{\lambda_2(\tau_1+\tau_3)} \quad (11)$$

Supporting Information Table 4. Optimized Parameter for the 4th order time correlation function.

Concentration of Mg^{2+}	τ_2 (waiting time)	A_{22}	A_{23}	A_{32}	A_{33}	Root Mean square error
50 mM	0.05 s	0.0391	0.0361	0.0361	0.0754	0.0278
	0.1 s	0.0374	0.0318	0.0318	0.0698	0.0272
	0.25 s	0.0346	0.0315	0.0315	0.0712	0.0250
	0.5 s	0.0311	0.0302	0.0302	0.0737	0.0222
200 mM	0.05 s	0.0430	0.0191	0.0191	0.0104	0.0029
	0.1 s	0.0325	0.0200	0.0200	0.0164	0.0036
	0.25 s	0.0382	0.0173	0.0173	0.0126	0.0033
	0.5 s	0.0348	0.0154	0.0154	0.0171	0.0045

Free Energy minima calculation[8]:

For a equilibrium process, the Gibbs free energy is given by $\Delta G^0 = -RTlnK$ where K is the equilibrium constant at temperature T. So here if we consider N number of microstates present in a system at a given

temperature T, then according to Boltzmann distribution the probability of i^{th} microstate was given by,

$$p_i = \frac{e^{-G_i/k_BT}}{\sum_{i=1}^{N} e^{-G_i/k_BT}} \quad (12)$$

where G_i represents as Gibbs free energy of the i^{th} microstate, and k_B was the Boltzmann constant. $\sum_{i=1}^{N} e^{-G_i/k_BT}$ was considered as partition function. Here we have considered probability density function of E_{FRET} was a sum of N macrostates $pE_{FRET} = \sum_{i=1}^{N} p_i(E_{FRET})$ present in the system which is unity. So, if we convert the free energy of microstate in terms E_{FRET} of then this will be,

$$\frac{G_i(E_{FRET})}{k_BT} = -\ln\left[p_i(E_{FRET})\right] \quad (13)$$

where $p_i(E_{FRET}) = A_i \exp^{[-E_{FRET}-\langle E_{FRET}\rangle_i]/2\sigma_i^2}$, $\langle E_{FRET}\rangle_i$ was mean FRET efficiency, A_i was amplitude and was the standard deviation.

Coarse-grained and All-atom Simulation Methodology

In order to access the structural ensemble of DNA HJ, we have employed a coarse-grained structure based model of nucleic acids with all-atom resolution. The potential energy function has been defined as

$$\begin{aligned} E = & \sum_{Bonds} k_{Bonds}(r_i - r_{i,0})^2 + \sum_{Angles} k_{Angles}(\theta_i - \theta_{i,0})^2 + \sum_{Impropers} k_{Impropers}\left(\chi_i - \chi_{i,0}\right)^2 \\ & + \sum_{Planars} k_{Planars}\left(\chi_i - \chi_{i,0}\right)^2 + \sum_{Backbone} k_{Backbone} F_D(\phi)\left(\phi_i - \phi_{i,0}\right) \\ & + \sum_{Contacts} \varepsilon_C\left[\left(\frac{\sigma_{ij}}{r_{ij}}\right)^{12} - 2\left(\frac{\sigma_{ij}}{r_{ij}}\right)^{6}\right] \\ & + \sum_{Non-Contacts} \varepsilon_{NC}\left[\left(\frac{\sigma_{NC}}{r_{ij}}\right)^{12}\right] + K_{Coulomb} B(\kappa) \sum_{i,j} \frac{q_i q_j e^{-\kappa r_{ij}}}{\varepsilon_{Solvent} r_{ij}} \end{aligned}$$

Where, $F_D(\phi) = [1 - \cos(\phi)] + 0.5[1 - \cos(3\phi)]$ (14)

The first five terms represent bonded, angular, proper and improper dihedral potentials. $r_{i,0}, \theta_{i,0}, \chi_{i,0}, \phi_{i,0}$ represent equilibrium bond-length, angle, proper and improper dihedrals and backbone dihedrals respectively and has been obtained from provided structure. Short-range native interactions has been modelled as LJ potential whereas non-native ones interact with a purely repulsive interactions such that the atoms do not overlap on each other. σ_{ij} represents distance between atoms i and j centre of mass while being in contact and ε_C denotes contact strength. Electrostatics have been described with Debye-Hückel model.

The parameters were set to the following values:

$k_{Bonds} = \frac{50\varepsilon}{Å^2}, k_{Angles} = \frac{40\varepsilon}{rad^2}, k_{Impropers} = \frac{5\varepsilon}{rad^2}, k_{Planars} = \frac{20\varepsilon}{rad^2}, \varepsilon_{NC} = 0.1\varepsilon, \sigma_{NC} = 2.5Å, \varepsilon = 1.0$

Timestep of 0.0005 has been used for solving the Langevin dynamics. Simulations has been performed Gromacs version 515[10] while SMOG (structure based model for biomolecules)[11-14] has been used to generate the topology and coarse-grained (CG) structures. Solvent has been treated

as an implicit dielectric medium with dielectric constant 80. Divalent salt $MgCl_2$ has been introduced explicitly in addition to a 50mM NaCl implicit buffer. However due to coarse resolution of our model in the absence of solvent, we have calibrated charge of ions through the computation of radial distribution of ions around DNA HJ in our CG model and compared the same with all-atom explicit solvent 200ns simulation (production run) of HJ at 200mM $MgCl_2$ at temperature 300K.

For explicit solvent all-atom simulations, we have used Amber OL21 forcefield for DNA and SPC/E water with ions234lm_1264_spce parameter set for divalent Mg^{+2}. Octahedral box has been used where DNA HJ was placed such that any atom on DNA HJ stays at least 1.6 nm away from surface of the box. Equation of motions were integrated with a timestep of 2 fs in NPT ensemble for the production run.

Upon running coarse-grained simulations with gradually decreasing Mg^{+2} and Cl^- charges, we have observed the radial distribution of Mg^{+2} around HJ significantly matches with all-atom explicit solvent simulations for ionic charges of Mg^{+2} =1.2 and Cl^-=0.6 in our coarse-grained model (**Figure S1**). The electrostatic interactions between DNA HJ and ions and intra-DHJ repulsions has been quantified by Debye-Hückel continuum electrostatics[15] [Equation 14] q_i and q_j denote the charge of the i^{th} and j^{th} bead, inter-bead distance has been denoted as r_{ij}, $\varepsilon_{Solvent}$ denotes the solvent dielectric constant, and $K_{Coulomb} = 4\pi\varepsilon_0$ =332 kcal/mol. $B(\kappa)$ was dependent on salt concentration and the radius (a) of ions produced by the dissociation of the salt, and was given by $B(\kappa) = \frac{e^{\kappa a}}{1+e^{\kappa a}}$. According to Debye-Hückel theory, electrostatic interactions of an ion ranges upto a distance of the order of κ^{-1}, which is called Debye screening length. The Poisson-Boltzmann equation leads to the following relation of κ to ionic strength, $\kappa^2 = \frac{8\pi N_A e^2 \rho_A I}{1000 \varepsilon_{Solvent} k_B T}$; where N_A represent the Avogadro number, e is charge of an electron, ρ_A denotes solvent density, I represent ionic strength of the medium, k_B is the Boltzmann constant, and T is the temperature in reduced units. DNA HJ was placed in a cubic box of dimensions $15 \times 15 \times 15$ nm At each temperature and salt concentration, multiple independent trajectories has been generated solving Langevin equation in an NVT ensemble.

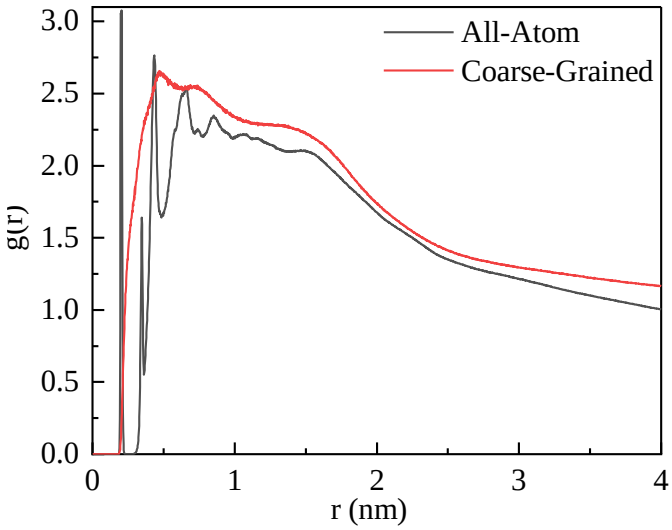

Figure S1. Radial distribution function of positively charged Mg^{2+} ions around negatively charged DNA HJ at near physiological salt concentration 200mM obtained from all-atom explicit solvent simulation with Amber forcefield and TIP4P water (black) and from coarse-grained structure based model in absence of solvent with continuum dielectric medium 80 (red).

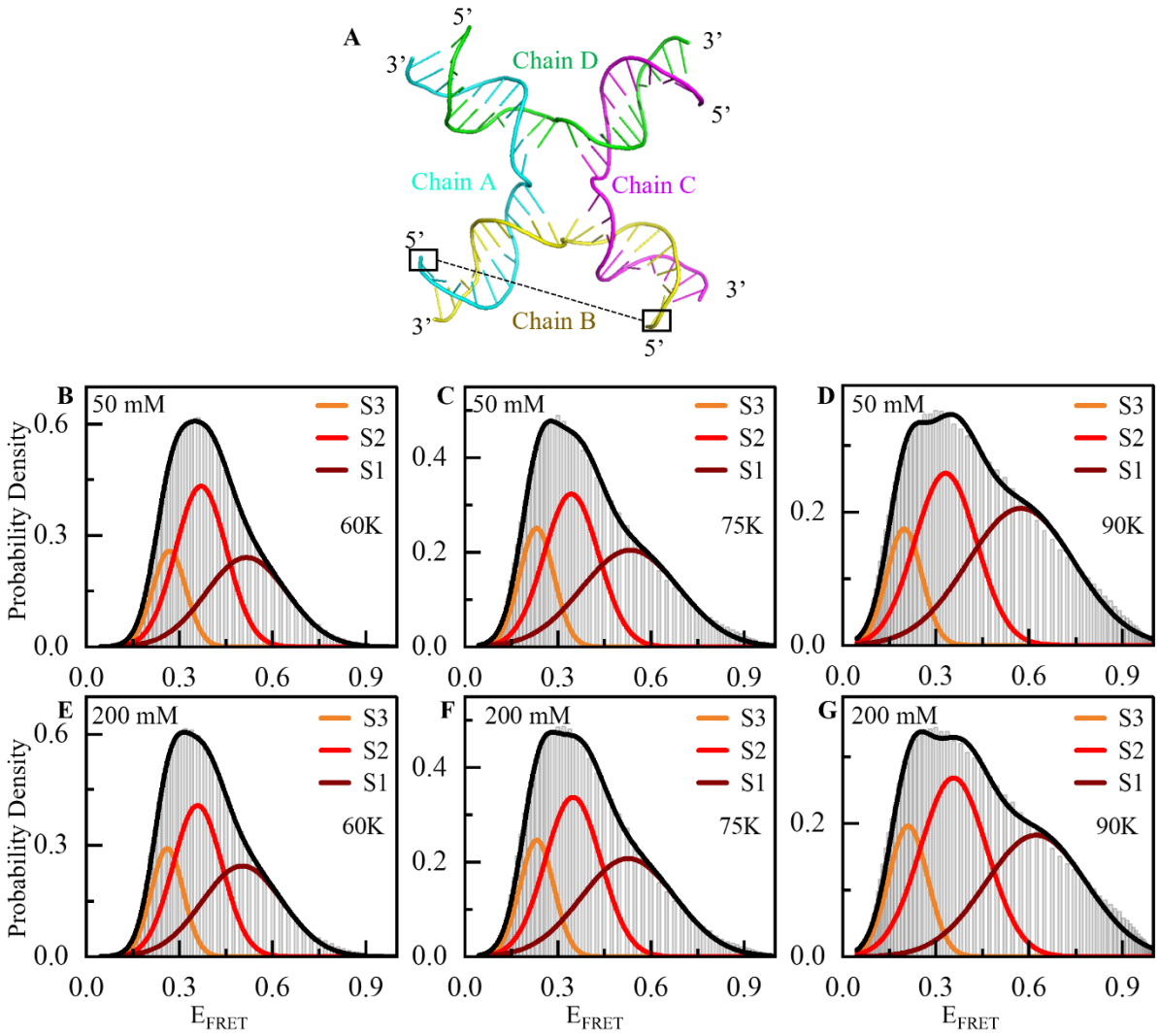

Figure S2.(A) Schematic diagram of Holliday junction shows that the FRET efficiency was calculated by considering the distance of chain A 5' position to chain B 5' position as per the **Supporting Information Table 1. (B-D)** Probability Density of FRET efficiency calculated from the MD simulation trajectory shows three prominent states corresponding to E_{FRET} in presence of 50 mM Mg^{2+} at 60K, 75K and 90K respectively. **(E-G)** Probability Density of FRET efficiency calculated from the MD simulation trajectory shows three prominent states corresponding to E_{FRET} in presence of 200 mM Mg2+ at 60K, 75K and 90K respectively.

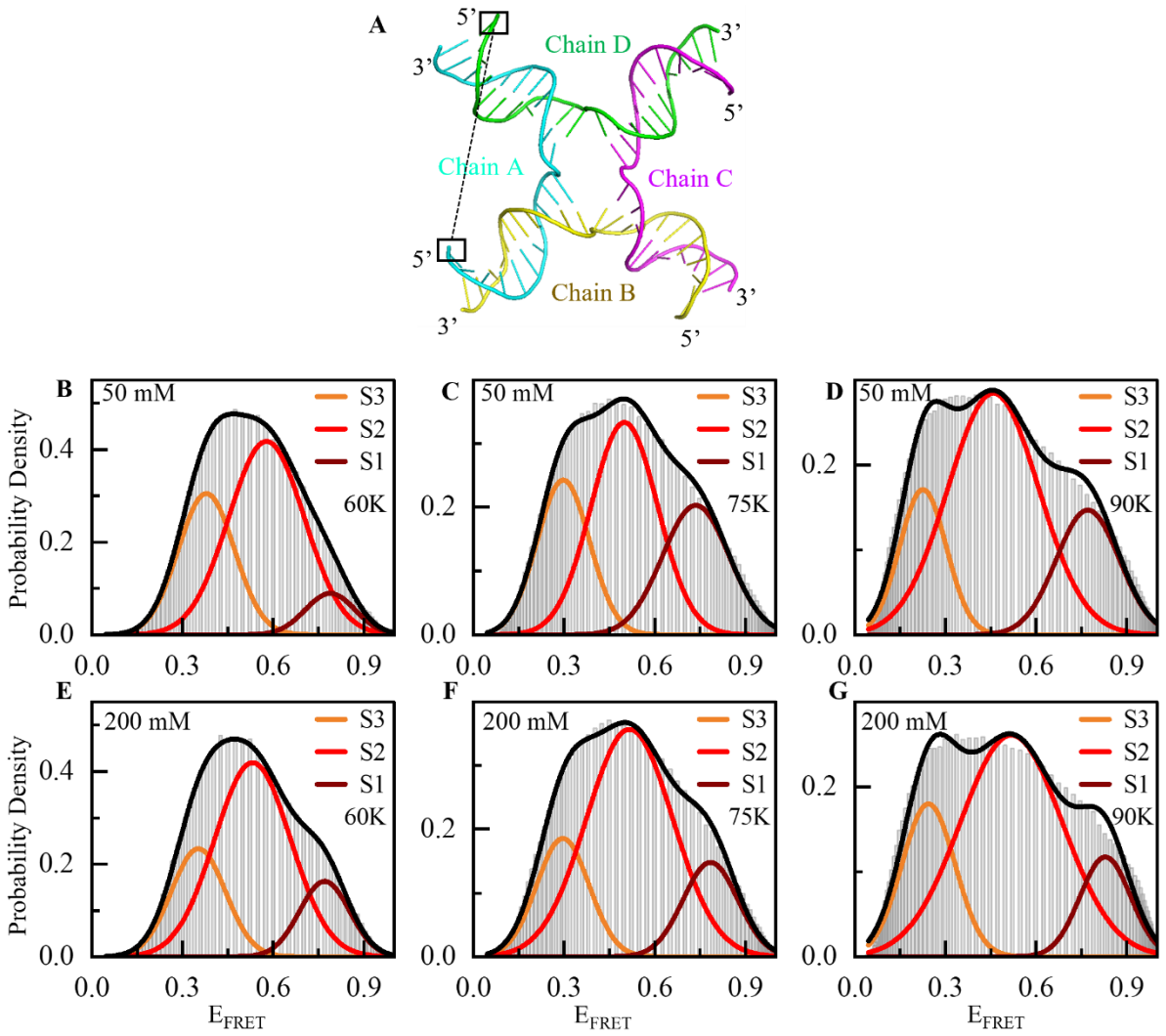

Figure S3. (A) Schematic diagram of Holliday junction shows that the FRET efficiency was calculated by considering the distance of chain A 5' position to chain D 5' position as per the **Supporting Information Table 1**. **(B-D)** Probability Density of FRET efficiency calculated from the MD simulation trajectory shows three prominent states corresponding to E_{FRET} in the presence of 50 mM Mg^{2+} at 60K, 75K and 90K, respectively. **(E-G)** Probability Density of FRET efficiency calculated from the MD simulation trajectory shows three prominent states corresponding to E_{FRET} in the presence of 200 mM Mg^{2+} at 60K, 75K and 90K, respectively.

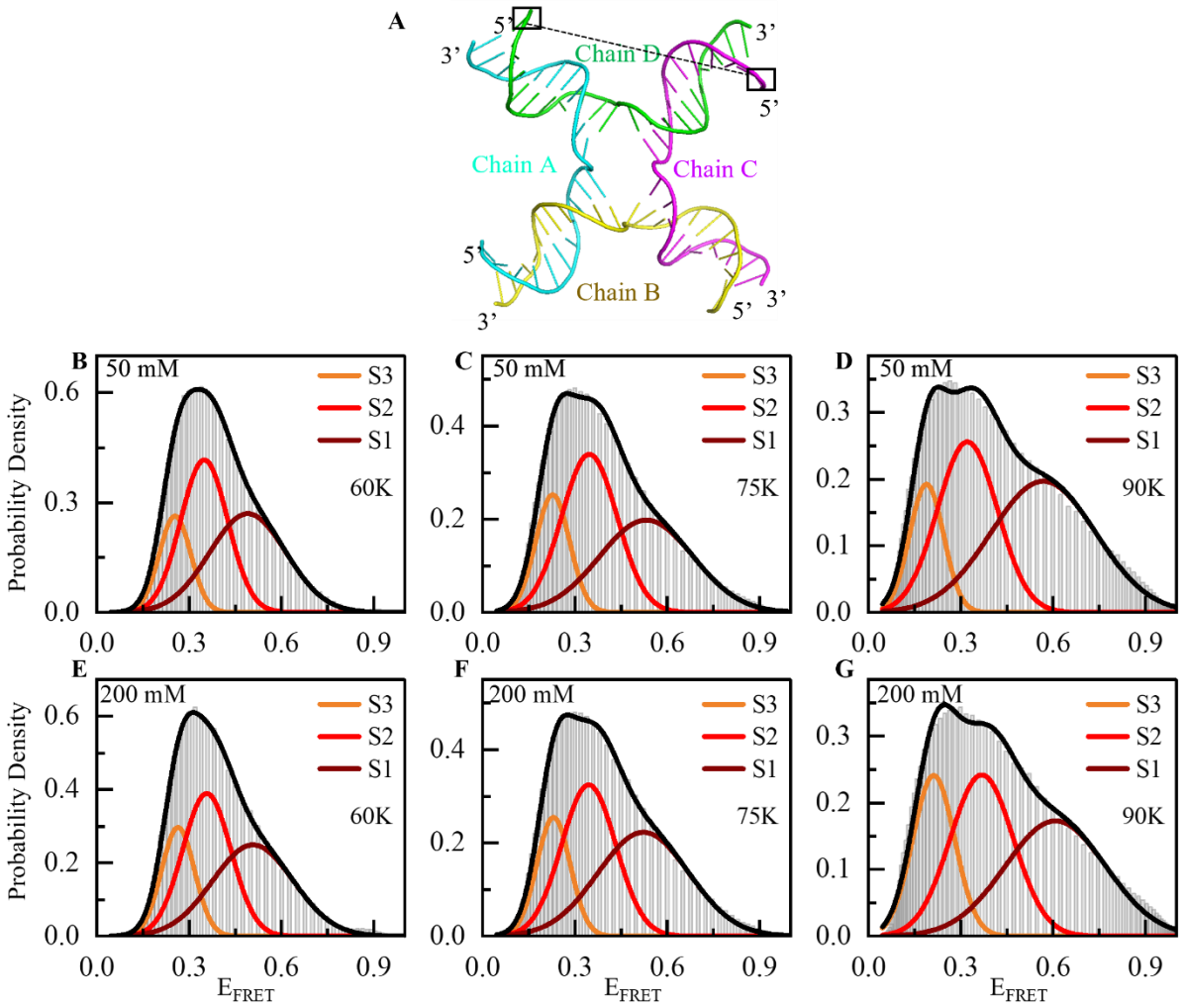

Figure S4. (A) Schematic diagram of Holliday junction shows that the FRET efficiency was calculated by considering the distance of chain C 5' position to chain D 5' position as per the **Supporting Information Table 1**. **(B-D)** Probability Density of FRET efficiency calculated from the MD simulation trajectory shows three prominent states corresponding to E_{FRET} in the presence of 50 mM Mg^{2+} at 60K, 75K and 90K, respectively. **(E-G)** Probability Density of FRET efficiency calculated from the MD simulation trajectory shows three prominent states corresponding to E_{FRET} in the presence of 200 mM Mg^{2+} at 60K, 75K and 90K, respectively.

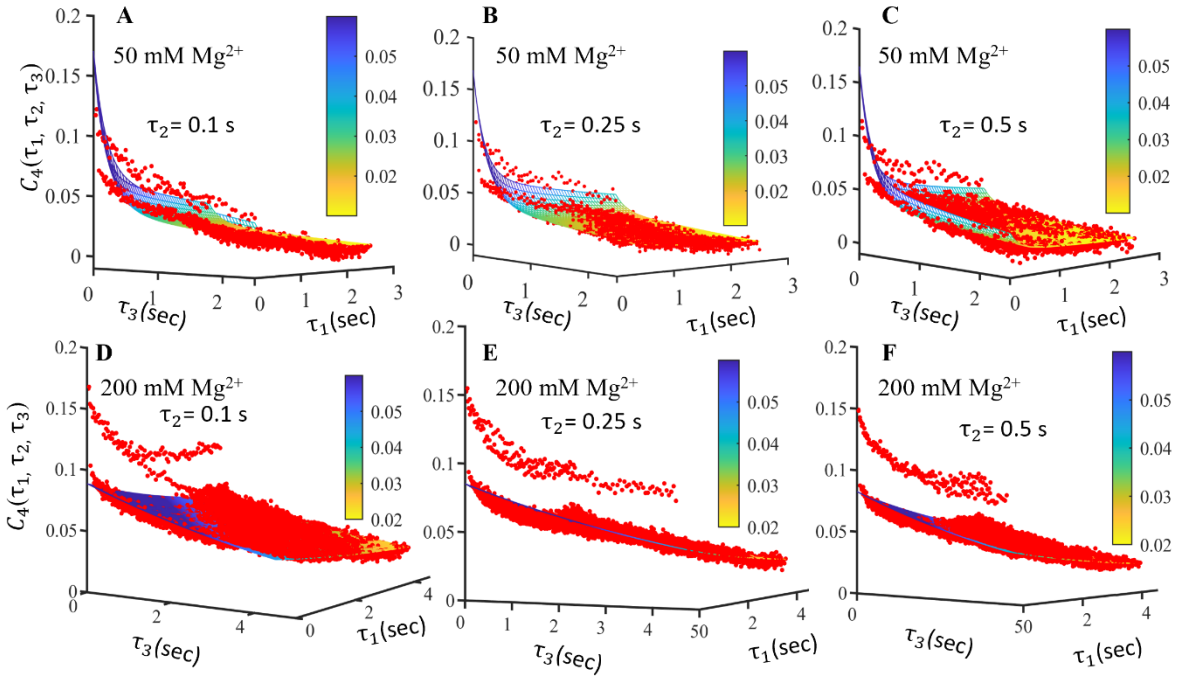

Figure S5. (A-C) Three-dimension plot of fourth order time correlation function at different waiting times 0.1 s, 0.25 s and 0.5 s, respectively, in the presence of 50 mM Mg^{2+}. **(D-F)** The three-dimension plot of the fourth order time correlation function at different waiting times 0.1 s, 0.25 s and 0.5 s respectively, in the presence of 200 mM Mg^{2+}.

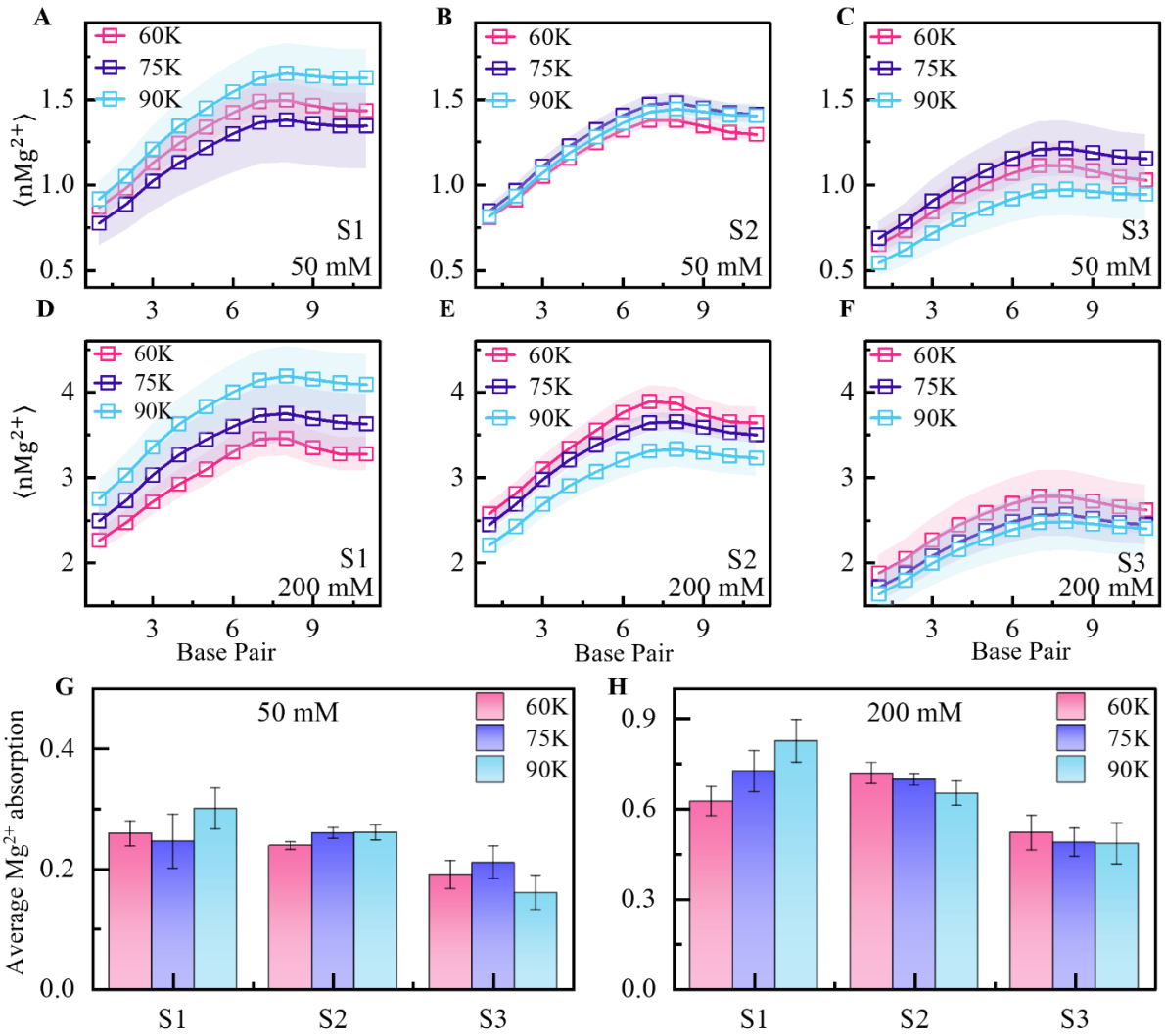

Figure S6. (A-C) Represents the number of Mg^{2+} vs the number of base pairs along the chain in a 1nm cylinder around each double strand of HJ in the presence of 50 mM Mg^{2+} concentration at 60K, 75K and 90K in state 1 (S1), State 2 (S2) and State 3 (S3) respectively. **(D-F)** Represents the number of Mg^{2+} vs the number of base pairs along the chain in a 1nm cylinder around each double strand of HJ in the presence of 200 mM Mg^{2+} concentration, at 60K, 75K and 90K in state 1(S1), State 2 (S2) and State 3 (S3) respectively. **(G-H)** Represents the average Mg^{2+} absorption for each double strand at 60K, 75K and 90K in State 1 (S1), State 2 (S2) and State 3 (S3), respectively, at 50 and 200 mM Mg^{2+}, respectively.

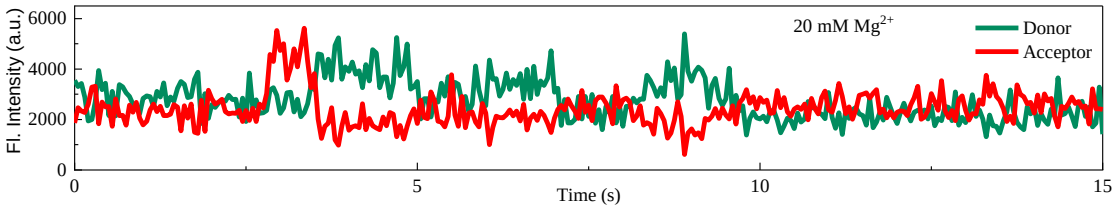

Figure S7. Representative single-molecule fluorescence intensity time-trajectories of Cy3 (Donor, Green) and Cy5 (Acceptor, Red) recorded from one single DNA Holliday junction in presence of 20 mM Mg^{2+} ion.

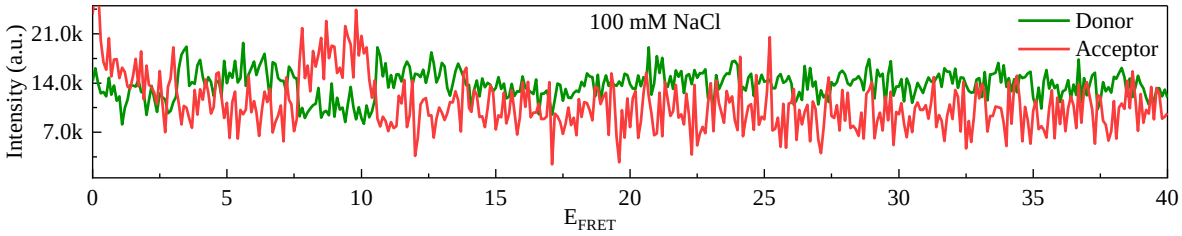

Figure S8. Representative single-molecule fluorescence intensity time-trajectories of Cy3 (Donor, Green) and Cy5 (Acceptor, Red) recorded from one single DNA Holliday junction in presence of 100 mM Na^+ ion.

Reference:

1. McKinney, S. A.; Déclais, A.-C.; Lilley, D. M.; Ha, T., Structural dynamics of individual Holliday junctions. *Nat. Struct. Biol.* **2003,** *10* (2), 93-97.
2. Joo, C.; Ha, T., Preparing sample chambers for single-molecule FRET. *Cold Spring Harbor Protocols* **2012,** *2012* (10), 1104-1108.
3. Joo, C.; Ha, T., Imaging and identifying impurities in single-molecule FRET studies. *Cold Spring Harbor Protocols* **2012,** *2012* (10), 1109-1112.
4. Gibbs, D. R.; Kaur, A.; Megalathan, A.; Sapkota, K.; Dhakal, S., Build your own microscope: step-by-step guide for building a prism-based TIRF microscope. *Methods Protoc.* **2018,** *1* (4), 40.
5. Edelstein, A. D.; Tsuchida, M. A.; Amodaj, N.; Pinkard, H.; Vale, R. D.; Stuurman, N., Advanced methods of microscope control using μManager software. *J. Microbiol. Methods* **2014,** *1* (2).
6. Juette, M. F.; Terry, D. S.; Wasserman, M. R.; Altman, R. B.; Zhou, Z.; Zhao, H.; Blanchard, S. C., Single-molecule imaging of non-equilibrium molecular ensembles on the millisecond timescale. *Nat. Methods* **2016,** *13* (4), 341-344.
7. Sasmal, D. K.; Pulido, L. E.; Kasal, S.; Huang, J., Single-molecule fluorescence resonance energy transfer in molecular biology. *Nanoscale* **2016,** *8* (48), 19928-19944.
8. Israels, B.; Albrecht, C. S.; Dang, A.; Barney, M.; von Hippel, P. H.; Marcus, A. H., Submillisecond Conformational Transitions of Short Single-Stranded DNA Lattices by Photon Correlation Single-Molecule Förster Resonance Energy Transfer. *J. Phys. Chem. B* **2021,** *125* (33), 9426-9440.
9. Phelps, C.; Israels, B.; Marsh, M. C.; von Hippel, P. H.; Marcus, A. H., Using multiorder time-correlation functions (TCFs) to elucidate biomolecular reaction pathways from microsecond single-molecule fluorescence experiments. *J. Phys. Chem. B* **2016,** *120* (51), 13003-13016.
10. Pronk, S.; Páll, S.; Schulz, R.; Larsson, P.; Bjelkmar, P.; Apostolov, R.; Shirts, M. R.; Smith, J. C.; Kasson, P. M.; Van Der Spoel, D., GROMACS 4.5: a high-throughput and highly parallel open source molecular simulation toolkit. *Bioinformatics* **2013,** *29* (7), 845-854.
11. Whitford, P. C.; Noel, J. K.; Gosavi, S.; Schug, A.; Sanbonmatsu, K. Y.; Onuchic, J. N., An all-atom structure-based potential for proteins: bridging minimal models with all-atom empirical forcefields. *Proteins: Struct., Funct., Bioinf.* **2009,** *75* (2), 430-441.
12. Noel, J. K.; Whitford, P. C.; Onuchic, J. N., The shadow map: a general contact definition for capturing the dynamics of biomolecular folding and function. *J. Phys. Chem. B* **2012,** *116* (29), 8692-8702.
13. Noel, J. K.; Levi, M.; Raghunathan, M.; Lammert, H.; Hayes, R. L.; Onuchic, J. N.; Whitford, P. C., SMOG 2: a versatile software package for generating structure-based models. *PLoS Comput. Biol.* **2016,** *12* (3), e1004794.
14. Clementi, C.; Nymeyer, H.; Onuchic, J. N., Topological and energetic factors: what determines the structural details of the transition state ensemble and “en-route” intermediates for protein folding? An investigation for small globular proteins. *J. Mol. Biol.* **2000,** *298* (5), 937-953.
15. Givaty, O.; Levy, Y., Protein sliding along DNA: dynamics and structural characterization. *J. Mol. Biol.* **2009,** *385* (4), 1087-1097.